Wavelet-based high order spectrum for local damage diagnosis of gears under different operating conditions

Rui ZHU[1,2], Georgios MOUSMOULIS[1,2], Konstantinos GRYLLIAS [1,2]

[1]LMSD Division Mecha(tro)nic System Dynamics, Department of Mechanical Engineering, KU Leuven, Celestijnenlaan 300, Box 2420, 3001 Leuven, Belgium
[2]Flanders Make@KU Leuven, Belgium
rui.zhu@kuleuven.be

Abstract

Gears play an important role in transmission systems, allowing for high performance in terms of load capacity and efficiency. Common gear faults such as cracked teeth and pitted teeth, can occur as a result of contact fatigue, excessive load, or sudden impact. Starting from an initial stage, their steady growth can lead to irreparable damage and unexpected breakdowns that result in economic losses. Therefore, local tooth damage diagnosis of gears using advanced monitoring techniques is extremely important for the normal operation of drivelines and transmissions. The presence of local tooth damage produces transient impact in the vibration signals, which exhibit non-stationary and non-linear characteristics. Taking into account its ability to characterize the phase coupling between signal components caused by non-linearity, wavelet-based high order spectrum is considered to be effective to attain reliable fault-related features. Among others, wavelet bicoherence technology has been successfully applied to detect the artificially created gear faults under steady speed and load. However, in case the operating condition changes, the effectiveness of this method in detecting gear faults is still unclear. Additionally, the selection of the informative bi-frequency bands and the extraction of instantaneous diagnostic features is still a challenge. This may constraint the widespread application of wavelet-based high order spectrum in gear fault diagnosis. This paper presents a novel strategy for selecting informative bi-frequency bands and extracting instantaneous diagnostic features in the time bi-frequency domain. The performance of the proposed methodology is evaluated by comparison with the WIF method and is extended to cases involving healthy and faulty gears operating under different speeds and loads. To validate the effectiveness of the methodology, an experimental dataset with artificially made gear pitting damage and a publicly available dataset which includes gears with various crack severity as well as different speed and load operating conditions is utilized.

1 Introduction

Gearboxes are extensively used in various industries for power transmission. However, the occurrence of unforeseen gear failures, such as local teeth defects like pitting, spalling, and cracks, can lead to costly breakdowns and substantial economic losses. Therefore, implementing condition monitoring is crucial to ensure operational safety and minimize expenses. Over the past several years, vibration-based diagnosis has been considered as a powerful and effective tool [1-3].

When local damage such as pitting exists on a gear tooth, it results in transient impulses each time the damaged surface meshes with other teeth [4]. Similarly, in the case of gear tooth cracks, the meshing process causes the cracked tooth to ‘open’ and ‘close’, leading to the breathing effect of the crack, which also produces sharp transients in the vibration signature [5]. The vibration signals generated during the meshing process of a gear tooth with local tooth damage exhibit characteristics of non-stationarity and non-linearity [6]. Consequently, conventional linear representations, such as the Short-Time Fourier Transform and the Continuous Wavelet Transform (CWT), prove less effective in capturing the complex nature of these signals.

The use of high-order spectra, such as bispectrum and bicoherence, has proven successful in identifying phase coupling and nonlinear behavior [7] in various fields like ocean engineering [8] and biomedical engineering [9]. Recently, these techniques have been introduced in the domain of condition monitoring and fault diagnosis of mechanical systems. For instance, Rivola et al. [10] employed the normalized bispectrum to detect cracks in beams, presenting high sensitivity to fatigue cracks. Bicoherence was applied in [11] to analyse vibration and acoustic signals acquired from a gearbox with artificially created broken teeth, yielding reliable fault-related information. Additionally, the combination of wavelet transform and bicoherence analysis, known as wavelet bicoherence (WB), has been proposed and utilized. More specifically, WB was employed in [12] for the detection of naturally-developing gear faults. To enhance accuracy, Li et al. [13] incorporated a biphase randomization step in WB and extracted two diagnostic features for bearing diagnostics of inner race defects.

However, the mentioned papers estimated WB by integrating over finite-time intervals, which may result in information loss in the time domain. To address this, the concept of instantaneous wavelet bicoherence/bispectrum (IWBC/IWBS) was introduced, enabling analysis in the time-bi-frequency domain. One notable application is in [6], where IWBC was employed for detecting multiple 'like natural' pitting faults in a back-to-back industrial spur gearbox system. Additionally, to preserve phase information, the instantaneous biphase randomization wavelet bicoherence was further developed by [14], successfully detecting chipped gear teeth and broken teeth.

Moreover, a challenge remains in the selection of informative bi-frequency bands to extract instantaneous diagnostic features in the time-bi-frequency domain. Currently, researchers mainly rely on information provided by the scalogram of CWT or make comparisons between healthy and faulty cases, which may not be convenient or accurate in certain scenarios. Thus, there is no mature approach for selecting/optimizing informative bi-frequency bands specifically related to faults in the time-bi-frequency domain in order to better extract the instantaneous diagnostic features.

Furthermore, in the application of wavelet-based high-order spectrum in condition monitoring area, the focus has primarily been on specific operating conditions. The effectiveness of the methodologies in detecting faults under changing operating conditions remains unclear.

The primary objective of this paper is to propose a novel diagnostic feature, the Enhanced Instantaneous Wavelet Bispectrum Feature (EIWBSF), for gear diagnostics. This is achieved by applying the instantaneous wavelet bispectrum and developing an optimization procedure for the informative frequency band. To validate the proposed methodology, vibration signals acquired from an experimental setup at KU Leuven are utilized, and the performance is compared with the classical WIF method [15]. Subsequently, a publicly available dataset including three severities of cracked gear tooth under different speed and load conditions is employed to test the effectiveness of EIWBSF in different operating conditions. The rest of the paper is organized as follows. In Section 2, the background theory is described while in Section 3, the proposed methodology is briefly presented. Moreover, in Section 4 the proposed EIWBSF is applied on the two datasets and the results are discussed. The paper's conclusions are then summarized in Section 5.

2 Basic signal processing theory

The forms of wavelet-based higher-order spectra rely on the utilization of CWT to process signals. CWT is a commonly used technique for characterizing the properties of non-stationary signals in the time-frequency domain. The CWT of a signal $x(t)$ can be presented by:

$$W_\psi(a,\tau) = \frac{1}{\sqrt{a}} \int_{-\infty}^{\infty} x(t) \psi^* \left(\frac{t-\tau}{a}\right) dt \tag{1}$$

where $\psi(t)$ is the mother wavelet function, a is the scale which can also be converted to frequency f, τ is the time shift variable, and $*$ represents the complex conjugation form.

The wavelet bispectrum (WBS) was initially introduced in the field of turbulence analysis and is defined as follows [16]:

$$B_{W,T}(f_1,f_2) = E\left\{\int_0^T W_\psi(f_1,\tau)\, W_\psi(f_2,\tau) W_\psi^*(f_3,\tau) dt\right\} \tag{2}$$

$W_\psi(f,\tau)$ is the wavelet coefficient calculated by the CWT of the signals, T is the time interval of the signal, $E\{.\}$ is the expectation operator. Additionally, the frequencies in the equation (2) satisfy the relationship of $f_3 = f_1 + f_2$.

Considering that the values of WBS are complex, WBS can be expressed in the form of amplitude $Amp(f_1, f_2)$ and biphase $\varphi(f_1, f_2)$ as following:

$$B_{W,T}(f_1, f_2) = E\{Amp(f_1, f_2)e^{i\varphi(f_1,f_2)}\} \tag{3}$$

$$\varphi(f_1, f_2) = \varphi(f_1) + \varphi(f_2) - \varphi(f_3) \tag{4}$$

where, $\varphi(f_1)$, $\varphi(f_2)$, and $\varphi(f_3)$ are respectively the phases of the frequencies f_1, f_2, f_3.

If the phase coupling exists in the signal, the phase component will satisfy the relationship:

$$\varphi(f_3) = \varphi(f_1) + \varphi(f_2) \tag{5}$$

and therefore the biphase $\varphi(f_1, f_2)$ will equal to 0. Thus $B_{W,T}(f_1, f_2) = E\{Amp(f_1, f_2)\}$, and the normalized version wavelet bicoherence (WBC) will be equal to 1.

In the case of non-phase coupling in the signal, the biphase $\varphi(f_1, f_2)$ is normally randomly distributed within (-π,π], which means that $e^{i\varphi(f_1,f_2)}$ is distributed within (-1,1]. Consequently, after taking the expectation operator, $B_{W,T}(f_1,f_2)$ tends to approach 0. As a result, the WBC approximates to 0.

Due to the fact that WBS and WBC need to be integrated over a finite-time interval, which may bring time information loss of the nonstationary signal, the IWBS has been proposed [6]. The IWBS aims to extend the bi-frequency domain to the time bi-frequency domain I and is defined as follows:

$$IWBS_{W,T}(f_1, f_2, \tau) = E\{W_\psi(f_1, \tau)W_\psi(f_2, \tau)W_\psi^*(f_3, \tau)\} \tag{6}$$

The IWBS can be further expressed by its instantaneous amplitude and biphase components, similar to the WBS, following the same rule for detecting the phase coupling and non-phase coupling part in the signals.

3 Proposed methodology

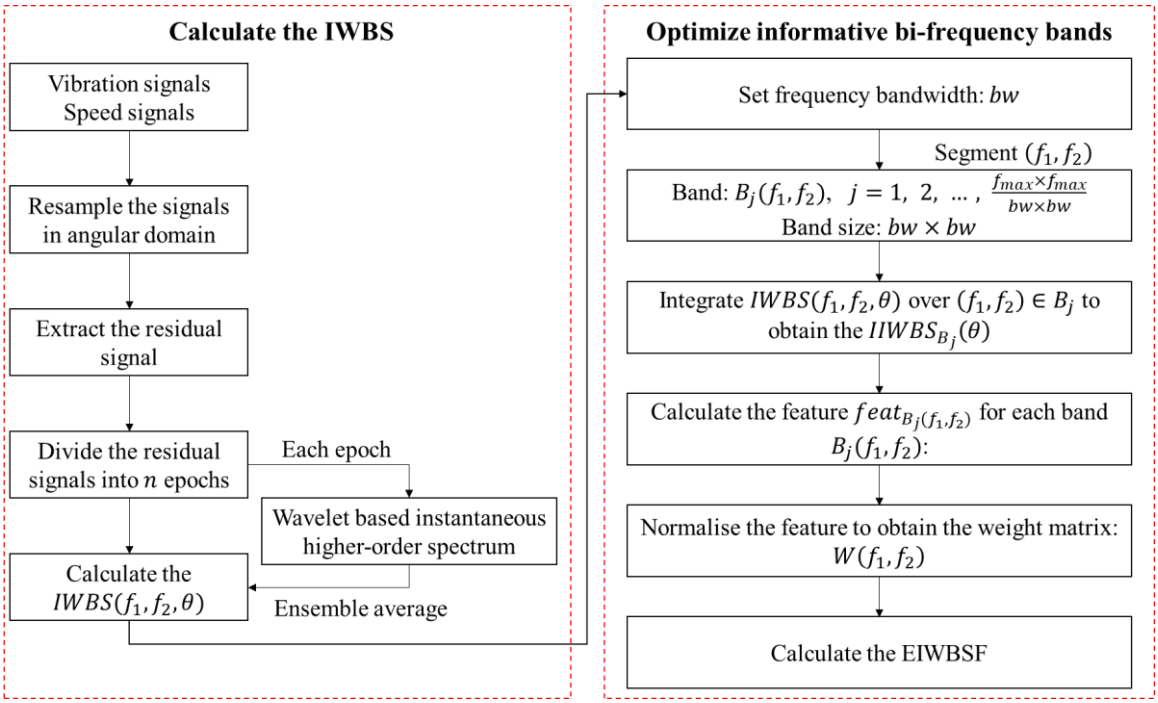

Figure 1: Schematic description of the EIWBSF

As mentioned before, the selection/optimization of informative bi-frequency bands to extract instantaneous diagnostic features in the time-bi-frequency domain is still challenging. To address this, the EIWBSF is proposed in this paper and presented in Figure 1. The specific steps are detailed in the following:

Step 1: Resample the raw vibration signal in the angular domain based on the speed signals.

Step 2: Estimate and remove the periodic part (e.g. mesh harmonic components) from the vibration signals to obtain the residual signals.

Step 3: Divide the vibration signal into n epochs based on the rotating period of the target gear, each epoch equals to one rotation period of the gear.

Step 4: Compute the IWBS of each epoch by equation (6).

Step 5: Obtain the $IWBS(f_1,f_2,\theta)$ by the ensemble average of IWBS of n epochs

Step 6: Segment the bi-frequency (f_1,f_2) into a series of bi-frequency bands $B_j(f_1,f_2)$, which has the band size $bw \times bw$, bw being the bandwidth.

Step 7: In each bi-frequency band, integrate the $IWBS(f_1,f_2,\theta)$ modulus over both frequencies f_1 and f_2 and obtain the $IIWBS_{B_j}(\theta)$ by equation (7).

$$IIWBS_{B_j}(\theta) = \frac{1}{B_j}\int\int |IWBS(f_1, f_2, \theta)|\, df_1 df_2 \tag{7}$$

Step 8: Extract the feature $feat_{B_j(f_1,f_2)}$ of each processed $IIWBS_{B_j}(\theta)$ with equation (8). The feature is based on the assumption that if a gear has a damaged tooth, then in one rotation period of the gear, there will be a high-amplitude impulse during the time interval when the damaged tooth meshes other teeth. Therefore, the numerator of equation (8) calculates this high-amplitude impulse by searching for the maximum value of $IIWBS_{B_j}(\theta)$ and integrated around the position of maximum value with the interval of $\Delta\theta$ ($\Delta\theta$ can be set via dividing one rotation by the tooth number). And the denominator of equation (8) is calculated as the integration of $IIWBS_{B_j}(\theta)$ subtracting the numerator, which is considered as the noise level.

$$feat_{B_j(f_1,f_2)} = \frac{\int_{\theta_{max}-\Delta\theta/2}^{\theta_{max}+\Delta\theta/2} IIWBS_{B_j}(\theta)d\theta}{\int IIWBS_{B_j}(\theta)d\theta - \int_{\theta_{max}-\Delta\theta}^{\theta_{max}+\Delta\theta} IIWBS_{B_j}(\theta)d\theta} \tag{8}$$

Step 9: The $feat_{B_j(f_1,f_2)}$ is then normalized between 0 and 1 to generate the weight matrix as shown in equation (9). Within the $W(f_1,f_2)$, each bi-frequency has a weight value.

$$W(f_1, f_2) = \frac{feat - min(feat)}{max(feat) - min(feat)} \tag{9}$$

Step 10: The final step is to weight the $IWBS(f_1,f_2,\theta)$ based on the weight matrix and to integrate the weighted $IWBS(f_1,f_2,\theta)$ modulus over both frequencies f_1 and f_2 to obtain the EIWBSF:

$$EIWBSF(\theta) = \frac{1}{B}\int\int |IWBS(f_1, f_2, \theta) \times W(f_1, f_2)|\, df_1 df_2 \tag{10}$$

4 Experimental application and results

4.1 Case 1 – Healthy and pitting gear under two speed conditions

In the first case study of this paper, experiments were conducted using a back-to-back gearbox setup at KU Leuven. The experimental setup consists of several components, including an electric motor A, the test gearbox, a planetary gearbox, and a loading electric motor B, as shown in Figure 2 (up). The kinematic diagram of the test gearbox is shown in Figure 2 (left), providing the gear information. Speed signals are obtained by an encoder installed on the back side of motor A, while two accelerometers (PCB 352A24) are placed on the top surface of the test gearbox and on the input shaft side, as depicted in Figure 2 (right). Both motors are induction motors of 1,5 kW power with rated load and speed of 5 Nm and 2880 rpm, respectively.

Healthy and faulty gears are tested on the setup (Figure 3). The faulty gear has one tooth with 50% pitting damage which is artificially created by a MED machine. During the tests, two rotational speeds (speed of the

motor A that is equal to the input shaft speed of the test gearbox) have been considered, 1620 rpm (~27 Hz) and 2200 rpm (~37 Hz). Additionally, the torque applied by the motor B can be estimated by the torque percentage (the ratio of the torque developed by the motor and the nominal torque) from the drive, which is around 5 Nm. The signals were sampled at a sampling frequency of 51200 Hz and the duration of each acquisition was 5 s. More details can be found in [15].

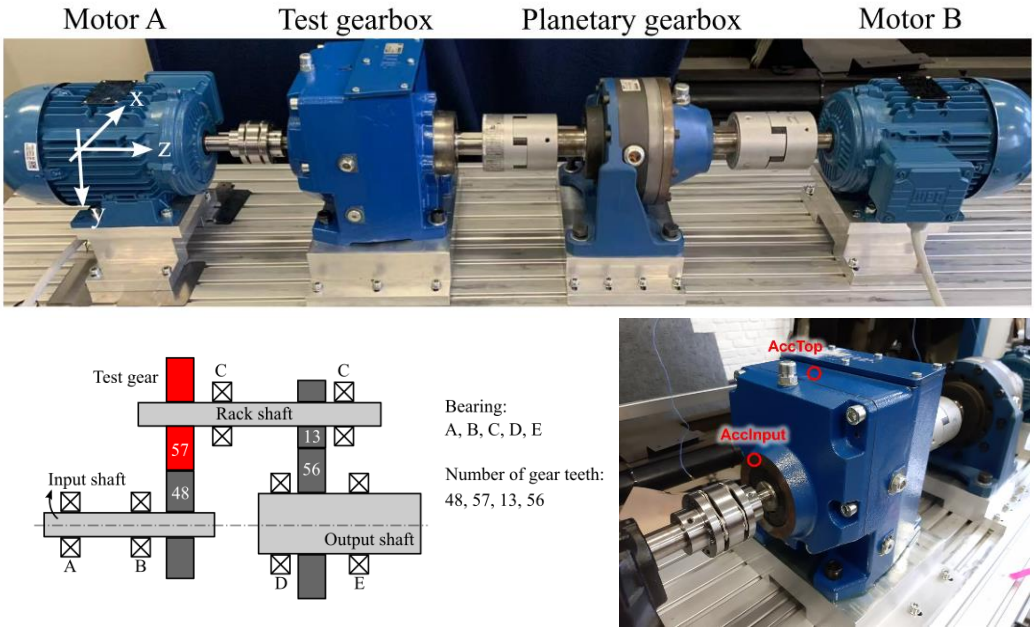

Figure 2: (up) The test rig setup, (left) the kinematic diagram of the test gearbox, (right) the accelerometers' position

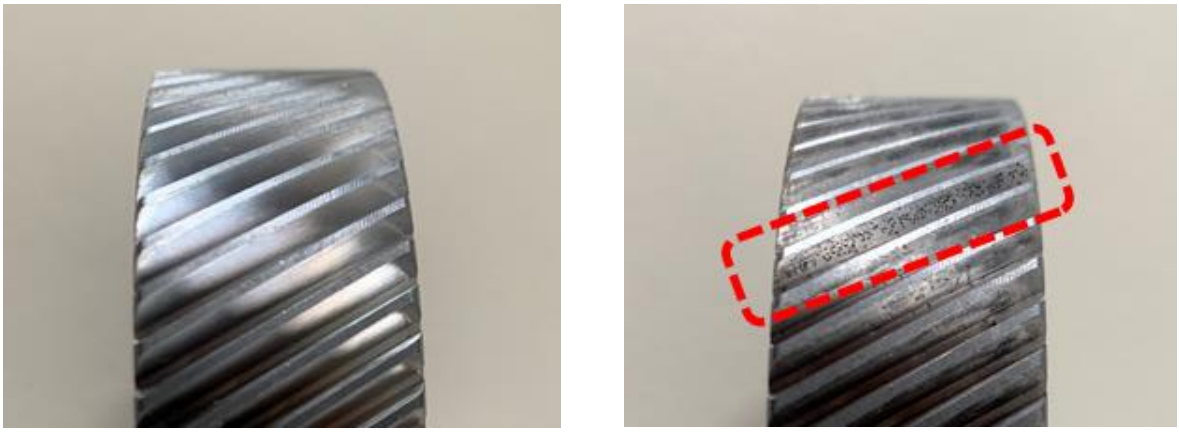

Figure 3: (left) Photo of the healthy gear, (right) photo of the faulty gear

For the case of speed 1620 rpm, raw vibration signals acquired from the accelerometer that is positioned close to the input shaft of the gearbox are used for analysis. The raw signals under healthy and faulty conditions are presented in Figure 4 (left). Besides, the residual signals extracted from the resampled signals by removing the periodic components are shown in Figure 4 (right). No apparent differences can be observed between the raw signals or the residential signals, as the fault information related to the impact produced by the tooth damage is very weak and is easy to be masked by the background noise.

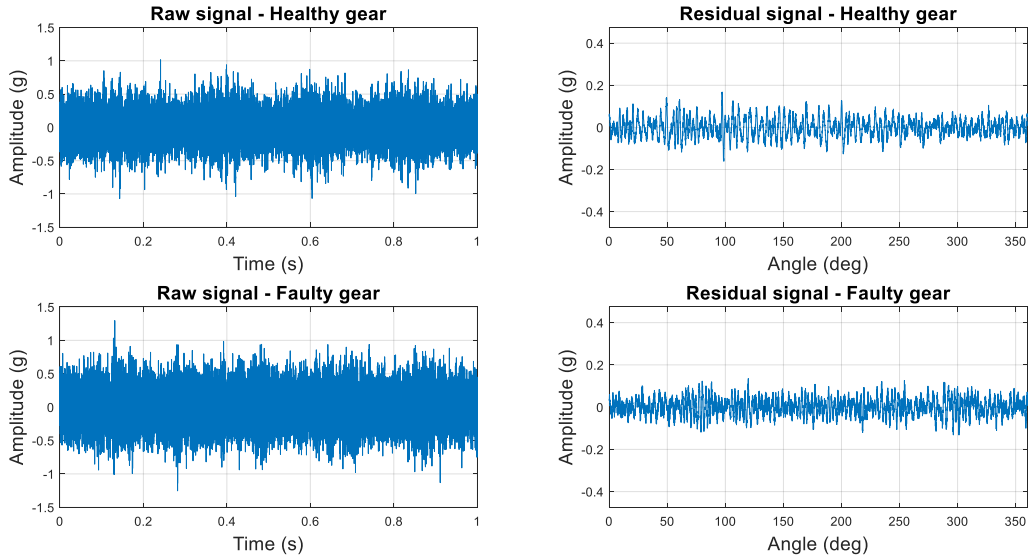

Figure 4: (left) The raw vibration signals, (right) residual signals of the healthy and faulty gear for 1620 rpm

Following the procedure described in Section 2, the IWBS of the healthy gear and the faulty gear is obtained by taking the ensemble average on the IWBS of the residual signals of all revolutions. As shown in Figure 5, the detected phase coupling of frequencies mainly exist within 200 orders. Comparing with the IWBS of the healthy gear, it is evident that the IWBS of the faulty gear exhibits a greater number of coupled frequencies in the time bi-frequency domain. This increase in coupled frequencies is attributed to the presence of pitting damage on the contact surface of the helical gear tooth.

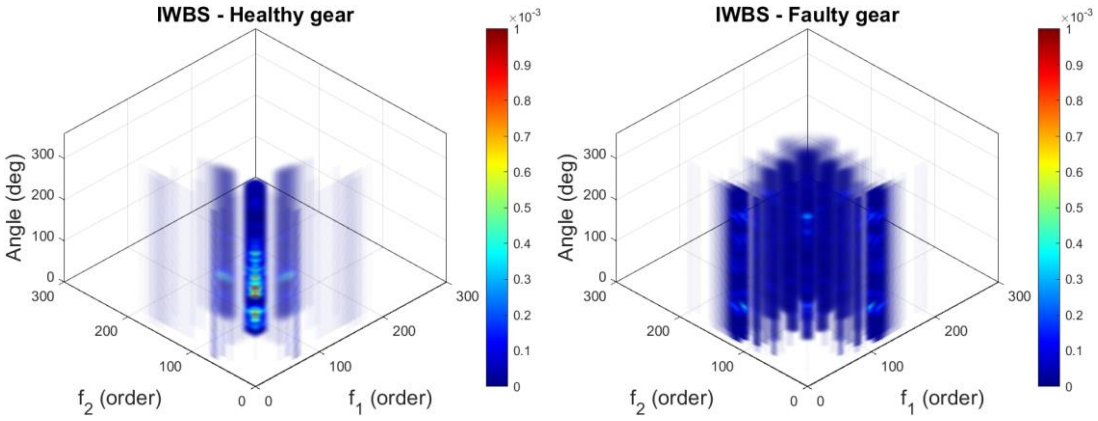

Figure 5: (left) IWBS of the healthy gear, (right) IWBS of the faulty gear for 1620 rpm

Considering the computing efficiency and the accuracy, the bandwidth was set based on the frequency resolution of the IWBS, thereafter the feature $feat_{B(f_1,f_2)}$ of each band was extracted, and the weight matrix of the bi-frequency band of the healthy and the faulty gear is displayed in Figure 6. From the results we can see the weight matrix exhibits high weight values around [73 order, 73 order] for both healthy and faulty gears. However, in the case of the faulty gear condition, additional high weight values can be observed in a different region, and more specifically, these high weight values are present in between the range of 100 ~ 150 order and 10 ~ 30 order. The presence of high weight values in the specific frequency region for the faulty gear case indicates that these regions are related to the pitting damage. This finding highlights the capability of the proposed feature to identify the fault-related informative band.

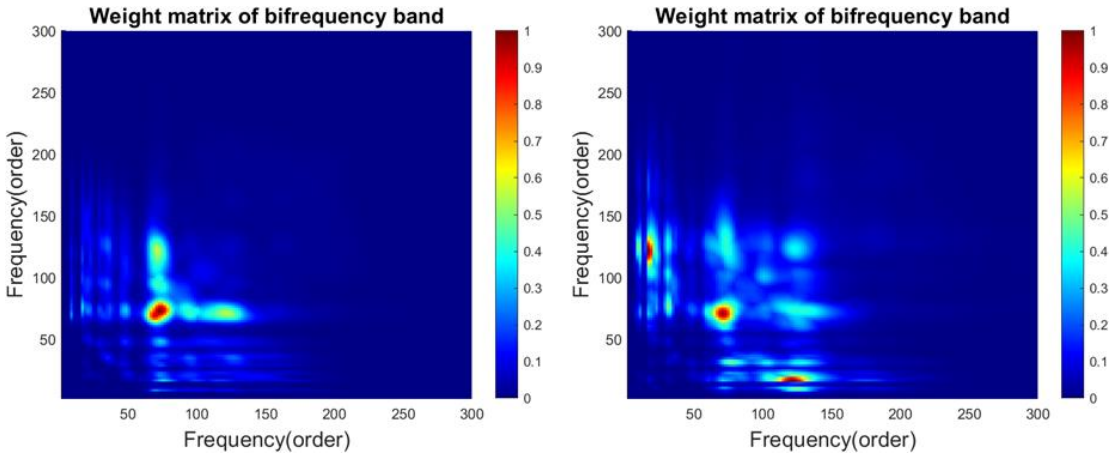

Figure 6: Weight matrix of IWBS (left) of the healthy gear, (right) of the faulty gear for 1620 rpm

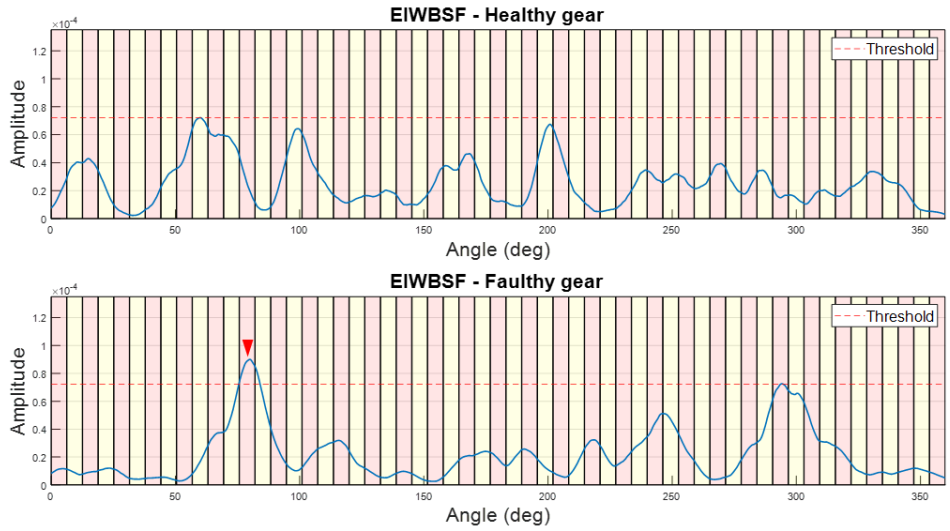

Figure 7: The EIWBSF of the healthy and the faulty gear for 1620 rpm

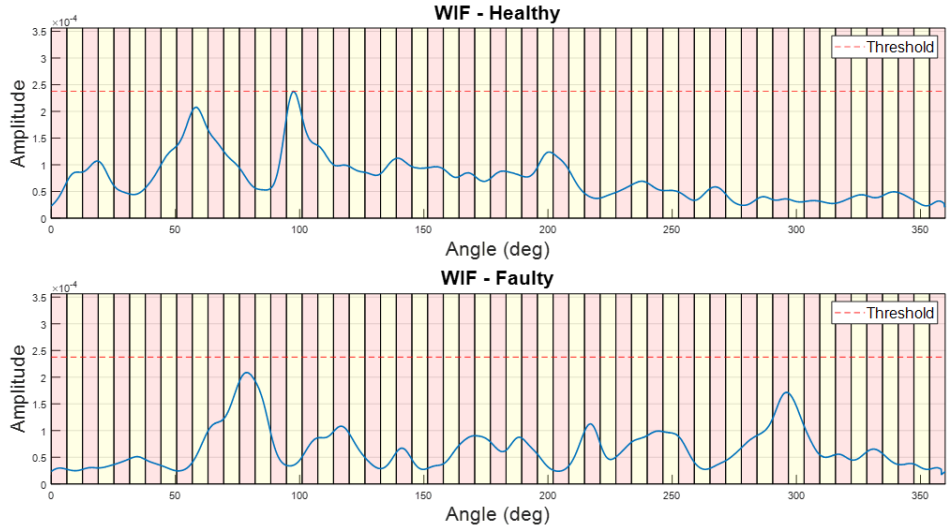

Figure 8: The WIF of the healthy and the faulty gear for 1620 rpm

Based on the results of Figure 5 and Figure 6, the EIWBSF is extracted using Equation 10. The corresponding EIWBSF results are presented in Figure 7, where the X-axis represents the angular position of

the gear, and the Y-axis represents the amplitude of the new feature. The maximum EIWBSF value of the healthy gear is set as the threshold to check if the faulty gear tooth can be detected. The vertical sections presented in the plots are drawn based on the assumption that there is no random fluctuation during the meshing process, thus, one rotation is divided into several intervals, each one corresponds to a specific gear tooth. From the results, it is clear that the EIWBSF of the faulty gear exceeds the threshold within a specific angle interval with the peak in the middle of the interval, which is around 80 deg.

In order to evaluate the proposed EIWBSF, it is compared with the WIF results presented in [15]. The threshold of the WIF is selected in the same way as in the EIWBSF case. From the results shown in Figure 8, the WIF of the faulty gear is always lower than the threshold extracted from the healthy gear, and it is concluded that the WIF methodology does not provide any valuable diagnostic information in this case, and consequently it cannot detect the pitting defect on the faulty gear.

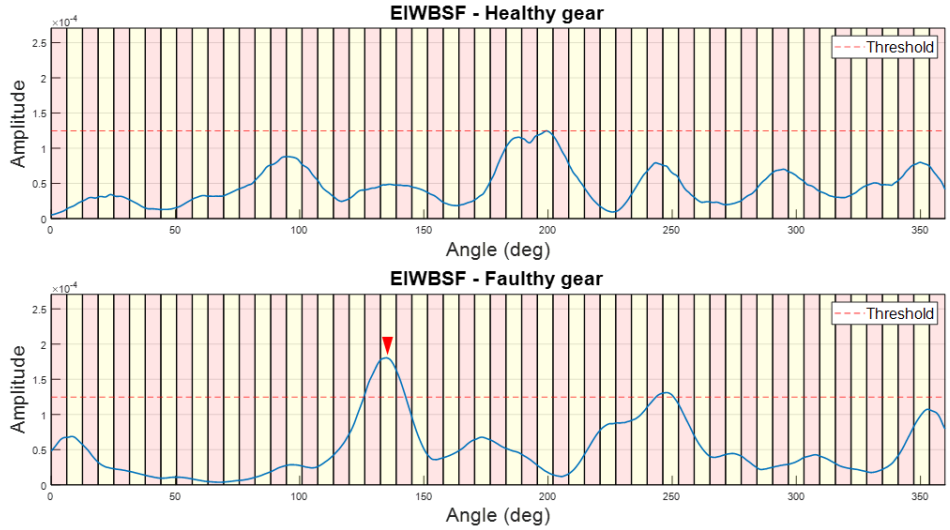

Figure 9: The EIWBSF of the healthy and the faulty gear for 2220 rpm

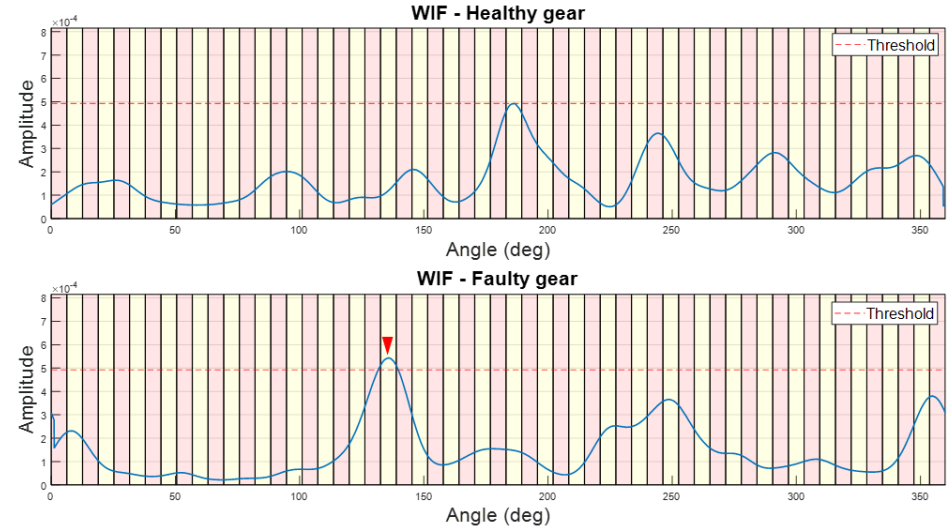

Figure 10: The WIF of the healthy and the faulty gear for 2220 rpm

Next, the case of operating speed at 2200 rpm is investigated. Figures 9 and 10 illustrate the WIF and the EIWBSF results obtained for both the healthy and faulty gears. The results indicate that both methodologies are capable of detecting the faulty gear tooth, as the maximum amplitude value of the diagnostic features exceed the threshold and peaked at around 135 deg. This is reasonable, as due to the higher speed conditions,

the impulses intensity caused by the mesh of pitted tooth become stronger, which consequently makes it easier to successfully detect the pitted tooth.

4.1 Case 2 – Cracked gear teeth under different speed and load conditions

The signals of the following case were acquired from the single-stage spur gearbox test rig presented in Figure 11. A 4-kW induction motor is connected to the input shaft. An electromagnetic particle (EMP) brake is connected to the output shaft to apply load to the rig. The gearbox consists of a 27-tooth driving gear and a 44-tooth driven gear. The encoders were mounted on the unloaded (free) end of both shafts with the resolution of 3600 pulses per shaft revolution. In addition, a torque meter is mounted in the input shaft to measure the input torque from the motor. Moreover two accelerometers are mounted on the gearbox for acquiring the vibration signals [17].

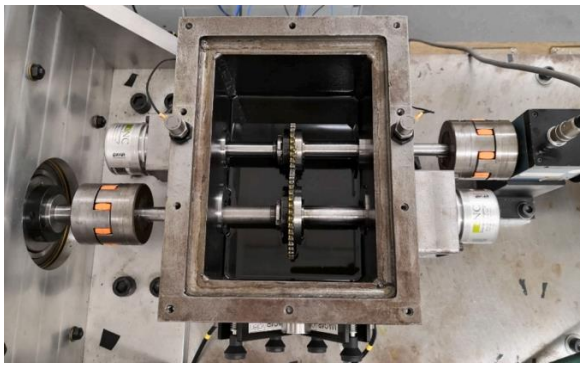

Figure 11: The single-stage spur gearbox test rig

A series of tests were conducted at different operating conditions, with pinion cracks of three different sizes (small, medium and large). To check the effectiveness of the proposed method under different speed and load conditions, the measurements collected at nominal input speeds of 10, 15 and 20 Hz and nominal loads of 10, 15 and 20 Nm are used, with the sampling frequency of 200 kHz and sampling duration of 21s.

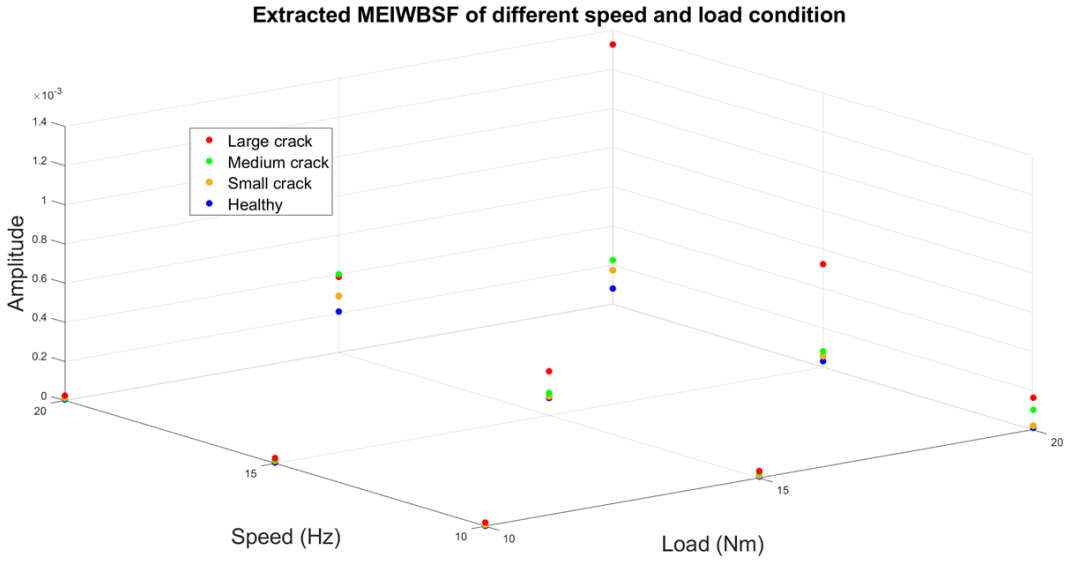

Figure 12: The MEIWBSF of the healthy, small crack, medium crack and large crack case at different speed and load

In order to check the effectiveness of the EIWBSF in detecting the faulty gears, the maximum value of EIWBSF (MEIWBSF) of gears under each operating condition is extracted as an indicator. The MEIWBSF corresponding to the healthy, small crack, medium crack and large crack gears are presented in Figure 12. For better visualization and comparison of the evolution of the faulty indicators in relation to the healthy

benchmark, a version of the MEIWBSF normalized by the healthy case is also plotted in Figure 13. The normalized MEIWBSF is just the indicator values divided by the healthy indicators for each load and speed conditions.

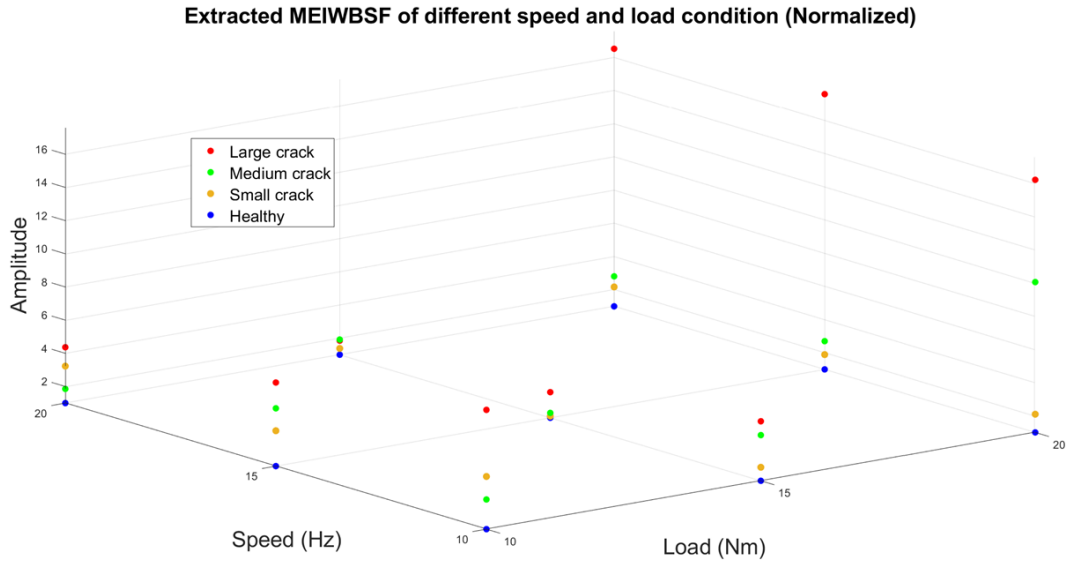

Figure 13: The normalized MEIWBSF of the healthy, small crack, medium crack and large crack case at different speed and load

The results of the MEIWBSF confirms the effectiveness of the EIWBSF in detecting faulty gear cases. The MEIWBSF values of the faulty gears, under different load and speed conditions, consistently exhibit higher values compared to the healthy gear. This observation is further emphasized in the normalized MEIWBSF results, where the deviation from the healthy benchmark becomes more significant.

Additionally, as the speed and load increase, the MEIWBSF values also show an upward trend. This correlation between the MEIWBSF values and the increase in speed and load is expected. Higher speeds and loads brings stronger impulses resulting from the breathing effect of the cracked tooth.

The normalized MEIWBSF results reveal valuable insights into the ability of MEIWBSF to detect fault severity. In most cases, the MEIWBSF values of the large crack case exhibit the highest values, followed by the medium crack case and then the small crack case. This trend aligns with the expected severity of the fault, indicating that MEIWBSF is capable of capturing and distinguishing different levels of damage.

However, it is worth noting that there are instances where the MEIWBSF of the small crack case appears higher than that of the medium crack case, which may occur because of the load being relatively low (i.e., 10 Nm). Therefore, repeatable experiments are needed to validate and ensure the consistency of the results, minimizing the experimental uncertainties and providing more reliable conclusions.

Nevertheless, a notable finding is that all the MEIWBSF values of the healthy cases are consistently lower than those of the faulty cases, ensuring that there are no missed detections.

5 Conclusion

This paper proposes a new diagnostic feature for the diagnosis of local damage in gears based on vibration signals. Initially, the acquired vibration signals are resampled in angular domain. Afterwards the residual signals are extracted by removing the periodical component from the resampled signals. Then, after segmenting the residual signal, the IWBS is obtained by ensemble average of IWBS of each epoch. An optimization of the informative bi-frequency band is proposed by a feature and the EIWBSF is obtained based on the weight matrix and integrations over the bi-frequency. To validate the methodology, an experimental dataset has been used, where a healthy gear and a faulty gear (one tooth with artificially generated 50% pitting damage) are tested under two operating speeds. By comparing with the classical WIF method, EIWBSF shows good performance in detecting the faulty gear tooth. Although WIF also works when operating the drivetrain at higher speeds, the EIWBSF shows to be able to extract the fault peaks more effectively, even under low

speed conditions. Additionally, the effectiveness of the methodology under different operating conditions is tested. A publicly available dataset is utilized, which includes gears with various crack severities as well as different speed and load conditions. The MEIWBSF is extracted as an indicator and the results show that the faulty cases can be successfully detected. Additionally in most of the case, the normalized MEIWBSF can distinguish clearly the severity of the gear fault. In the future, more tests will be done in order to validate and further improve the applicability of the method by considering the damage evolution, multi-teeth defects as well as various defect types.

Acknowledgments

Rui Zhu would like to gratefully acknowledge the support from the China Scholarship Council. This work was supported by Flanders Make, the strategic research center for the manufacturing industry, in the context of the QED project.

References

[1] C. Liu, Y. Meerten, K. Declercq, and K. Gryllias, *Vibration-based gear continuous generating grinding fault classification and interpretation with deep convolutional neural network*, J. Manuf. Process., 2022, pp.688–704.

[2] R. B. Randall, *Vibration-based Condition Monitoring: Industrial, Automotive and Aerospace Applications*, John Wiley & Sons, 2021.

[3] A. Mauricio, J. Qi, and K. Gryllias, *Vibration-Based Condition Monitoring of Wind Turbine Gearboxes Based on Cyclostationary Analysis*, J. Eng. Gas. Turbines Power-Trans. ASME, 2019 March, pp. 031026.

[4] L. Gelman, K. Soliński, and A. Ball, *Novel Higher-Order Spectral Cross-Correlation Technologies for Vibration Sensor-Based Diagnosis of Gearboxes*, Sensors, 2020 September, pp.5131.

[5] D. Peng, W. A. Smith, P. Borghesani, R. B. Randall, and Z. Peng, *Comprehensive planet gear diagnostics: Use of transmission error and mesh phasing to distinguish localised fault types and identify faulty gears*, Mech. Syst. Signal Proc., 2019 July, pp.531–550.

[6] F. Combet, L. Gelman, and G. LaPayne, *Novel detection of local tooth damage in gears by the wavelet bicoherence*, Mech. Syst. Signal Proc., 2012 January, pp.218–228.

[7] C. R. P. Courtney, S. A. Neild, P. D. Wilcox, and B. W. Drinkwater, *Application of the bispectrum for detection of small nonlinearities excited sinusoidally*, J. Sound Vibr., 2010 September, pp. 4279–4293.

[8] S. Zhang, J. Lian, J. Li, F. Liu, and B. Ma, *Wavelet bispectral analysis and nonlinear characteristics in waves generated by submerged jets*, Ocean Eng., 2022 November, pp.112473.

[9] L. J. Hadjileontiadis, *Continuous wavelet transform and higher-order spectrum: combinatory potentialities in breath sound analysis and electroencephalogram-based pain characterization*, Phil. Trans. R. Soc. A., 2018 August, pp.20170249.

[10] A. Rivola and P. R. White, *Bispectral analysis of the bilinear oscillator with application to the detection of fatigue cracks*, J. Sound Vibr., 1998 October, pp.889–910.

[11] V. Gunasegaran, M. Amarnath, H. Chelladurai, and I. R. P. Krishna, *Assessment of local faults in helical geared system using vibro-acoustic signals based on higher order spectrum analysis*, Appl. Acoust., 2023 March, pp.109237.

[12] L. Gelman, K. Solinski, B. Shaw, and M. Vaidhianathasamy, *Vibration diagnosis of a gearbox by wavelet bicoherence technology*, Insight, 2017 August, pp.440–444.

[13] Y. Li, J. Lin, X. Wang, and Y. Lei, *Biphase randomization wavelet bicoherence for mechanical fault diagnosis*, Measurement, 2014 March, pp.407–420.

[14] Y. Li and S. Zhou, *A New Instantaneous Wavelet Bicoherence for Local Fault Detection of Rotating Machinery*, IEEE Trans. Instrum. Meas., 2020 January, pp.135–143.

[15] R. Zhu, G. Mousmoulis, and K. Gryllias, *An enhanced wavelet-based instantaneous feature for local damage diagnosis of gears*, Proceedings of ISMA-USD2022 conference, Leuven, Belgium, 2022 September, pp.639-651.

[16] B. Ph. van Milligen et al., *Wavelet bicoherence: A new turbulence analysis tool*, Phys. Plasmas, 1995 August, pp.3017–3032.

[17] Z. Y. Chin, P. Borghesani, Y. Mao, W. A. Smith, and R. B. Randall, *Use of transmission error for a quantitative estimation of root-crack severity in gears*, Mech. Syst. Signal Proc., 2022 May, pp.108957.